

# Fast Numerical Method for Growth and Retreat of Subsurface Ice on Mars

Norbert Schorghofer

*Institute for Astronomy, 2680 Woodlawn Drive, University of Hawaii, Honolulu, HI 96822*

---

## Abstract

Subsurface water ice on Mars evolves due to exchange of vapor with the atmosphere, in the form of loss of ice to the atmosphere or in the form of the growth of interstitial ice. Described here is an accelerated numerical method for the long-term evolution of subsurface ice. This accelerated method is five orders of magnitude faster than explicit vapor transport calculations, enabling fundamentally new types of climate models. Its speed matches that of purely thermal models. The speedup is achieved primarily by solving time-averaged equations for vapor transport and ice volume change. Processes incorporated are growth of interstitial pore ice, retreat of pore ice, retreat of an ice sheet, and retreat of pore ice due to geothermal heating from below. Two example applications illustrate this numerical method's capabilities. Near the permafrost margin at 55 degrees latitude, ice is periodically depleted and slowly recharged, leading to a pore ice layer estimated to be currently no more than a few meters thick. At the Phoenix Landing Site, it shows the formation of a three layered structure, whereby the layer of pore ice can be very thin.

---

## 1. Introduction

Subsurface ice buried by a layer of dry soil is found at the Phoenix Landing site (Smith et al., 2009; Mellon et al., 2009; Sizemore et al., 2010) and over a significant part of Mars' surface (Boynton et al., 2002; Feldman et al., 2002; Mitrofanov et al., 2002). This ice rapidly exchanges vapor with the atmosphere (e.g., Mellon and Jakosky, 1993; Hudson et al., 2007). It represents a significant portion of the volatile ice volume on Mars globally, and it is thus an important component of long-term climate models that follow orbital variations.

Numerous authors (e.g., Flasar and Goody, 1976; Jakosky, 1983; Mellon and Jakosky, 1993, 1995; Schorghofer and Aharonson, 2005) have used diffusion models to study the interaction between atmospheric water vapor and ground ice. These computations involved diffusion of water vapor through the soil, sublimation from ice to vapor and vice versa, and some of these models also include physical adsorption

of H<sub>2</sub>O on the soil. The models are either based on a continuum description of vapor transport in form of a partial differential equation (e.g., Mellon and Jakosky, 1993; Schorghofer and Aharonson, 2005) or use discrete molecules (Clifford and Hillel, 1986; Mellon and Jakosky, 1993; Helbert and Benkhoff, 2003). Both types of models are capable of simulating Knudsen as well as Fickian diffusion, that is, the molecular mean free path can be longer or shorter than the pore size.

It is well-known that explicit numerical methods for the diffusion equation are subject to numerical stability requirements; the typical time step requirement is (e.g., Ames, 1992; Press et al., 1992)

$$\Delta t_{\text{expl.}} < \frac{\Delta z^2}{2D}, \quad (1)$$

where  $\Delta z$  is the vertical spatial resolution and  $D$  the diffusion coefficient. The vertical grid spacing needs to be finer than the diurnal skin depth of the temperature cycle. The diurnal skin depth is typically

a few centimeters to a decimeter on Mars. (This is a conservative estimate; physical adsorption of water molecules on the soil surface can restrict the breathing skin depth to much less than the thermal skin depth.) The diffusion coefficient has been measured in the laboratory for numerous Mars soil simulants (Hudson et al., 2007; Chevrier et al., 2007; Sizemore and Mellon, 2008; Hudson and Aharonson, 2008); it is typically  $D \approx 4 \times 10^{-4} \text{ m}^2/\text{s}$ . Thus, the time step needs to be smaller than  $\sim 0.01^2 / (2 \times 4 \times 10^{-4}) \approx 0.1 \text{ s}$ . This is a serious practical impediment for computations of ice evolution over long periods of Mars history.

Thermal models, which solve the heat conduction equation in the subsurface, can take advantage of implicit or semi-implicit numerical methods, such as the Crank-Nicholson method. In this case, the time step is only restricted by the requirement that the diurnal cycle be accurately resolved and may be tens of minutes ( $\sim 10^3 \text{ s}$ ). A vapor diffusion model, on the other hand, is intrinsically nonlinear, because of the phase transitions, and implicit methods can no longer be used. Hence, a vapor diffusion model is four orders of magnitude slower than a thermal model.

The key idea to overcome this limitation is the use of time-averaged transport equations (e.g. Schorghofer, 2007b). This method and its implementation are the subject of the present article. It was first used in Schorghofer (2007a) and is here developed further and described in detail. Before embarking on the mathematical description, Figure 1 shows a comparison between simulations of pore ice growth with a full microphysical model (Schorghofer and Aharonson, 2005) and the faster method described here. It shows the growth of interstitial pore ice after 50,000 years using an explicit vapor diffusion calculation and, for comparison, the solution of the time-averaged equation. The fast method does not reproduce seasonal subsurface frost, but correctly predicts the amount of perennial pore ice.

“Pore ice” refers to the ice within soil pores. Equivalently this layer may be described as ice-cemented soil, interstitial ice, or “icy dirt”. “Ice sheet” refers to pure or almost pure ice; it may also be thought of as “dirty ice”. “Excess ice” is the volume of ice in the ground which exceeds the total pore volume that

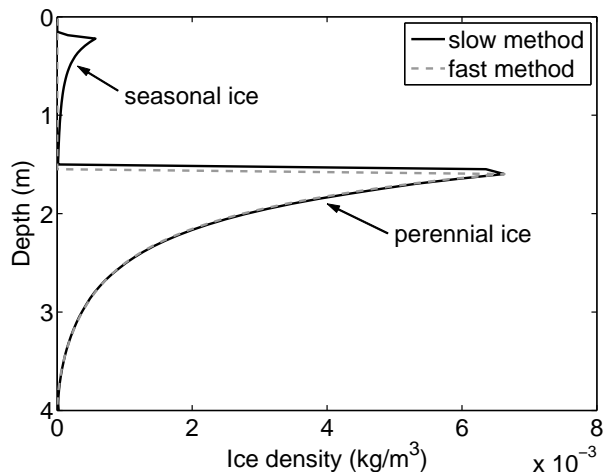


Figure 1: Model calculations where vapor from the atmosphere diffuses into the subsurface to form pore ice. Shown is the amount of pore ice after 50 ka as a function of depth below the surface, beginning with initially ice-free soil. The solid line is obtained from an explicit microphysical model, and the dash line from the accelerated numerical method. The fast method does not reproduce seasonal subsurface ice, but correctly predicts the amount of perennial ice. (An unrealistically small soil diffusivity was chosen to relax the time step requirement for the explicit model; thus the unrealistically small amount of ice after such a long time.)

the ground would have when ice-free. Upon loss of the ice, a soil containing excess ice settles under its own weight (van Everdingen, 1998). As used here, a layer of pore ice has no excess ice, while the ice sheet consists of a large portion of excess ice. Retreating pore ice leaves the soil matrix unchanged, while for a retreating ice sheet the overlying dry layer thickness grows more slowly, if at all. An ice sheet may form from precipitated snow and may be buried by its own sublimation lag, but other formation mechanisms are not excluded.

The evolution of subsurface ice involves one or the other of the following three processes: retreat of an ice sheet, retreat of pore ice, and the growth of pore ice. Every process involved needs to be treated with an accelerated method. The growth of an ice sheet (formation of excess ice) is not included, but an ice sheet can enter the calculation as initial condition. Figure 2 schematically shows the layering in the sub-

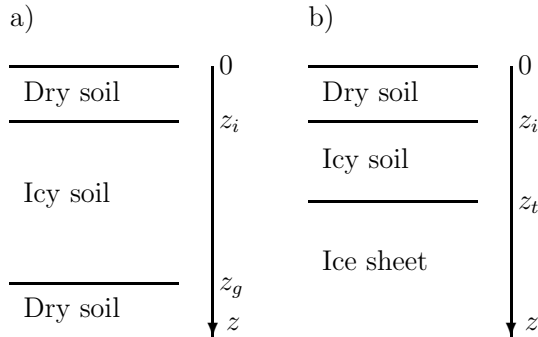


Figure 2: Schematic illustration of the vertical layering. The surface is at  $z = 0$ . The pore ice occupies depths either (a) from the interface depth  $z_i$  to a geothermally limited depth  $z_g$  or (b) from  $z_i$  to the depth of an ice table  $z_t$ .

surface in two situations. (a) In the absence of an ice sheet, pore ice extends from a depth  $z_i$  to the lower boundary of the numerical domain or until geothermal heat from below stops downward migration of  $\text{H}_2\text{O}$ . (b) An ice sheet underlies the soil.

The numerical grid is one-dimensional (vertical) and the same as for the underlying thermal model. It can have irregular grid spacing but is constant with time. Repeatedly used symbols are listed in Table 1. Time-averages are indicated with an overbar.

## 2. Growth of Interstitial Ice

When climate conditions are conducive to the stability of ice and the soil is permeable, ice will form in pore spaces by deposition of atmospheric water vapor. This has been predicted theoretically by Mellon and Jakosky (1993) and reproduced in laboratory experiments by Hudson et al. (2009). Among the variables that describe this process are the volumetric fraction  $f$  to which pore spaces are filled with ice,  $0 \leq f \leq 1$ , the diffusion coefficient in the ice-free porous medium  $D_{\text{dp}}$ , and the (mean annual) saturation vapor density  $\bar{\rho}_{sv}$ . The relation between filling fraction and the ice density  $\sigma$ , relative to total volume, is

$$f = \frac{\sigma}{\Phi_0 \rho_{\text{ice}}}. \quad (2)$$

### 2.1. Location of interface during growth

Detailed numerical model calculations by Schorghofer and Aharonson (2005) and laboratory experiments by Hudson et al. (2009) have shown that condensation of atmospherically derived ice in soil pores leads to accumulation of ground ice below a sharply defined interface. The depth  $z_i$  of this interface can be determined as follows.

The vapor flux between the surface and the interface is,

$$\bar{J}_{\text{dry}} = -D_{\text{dp}} \frac{\bar{\rho}_{sv}(z_i) - \bar{\rho}(0)}{z_i}, \quad (3)$$

where  $\bar{\rho}(0)$  is the mean annual water vapor density on the surface. Below the interface, the diffusive flux is governed by the saturation vapor pressure,

$$\bar{J}_{\text{sat}} = -D_{(\text{icy layer})} \frac{\partial \bar{\rho}_{sv}}{\partial z}. \quad (4)$$

The diffusion coefficient in the icy layer depends on the filling fraction and may be written in terms of an obstruction function  $\eta$ , such that

$$D_{(\text{icy layer})} = \eta D_{\text{dp}}, \quad (5)$$

where  $\eta(z)$  can vary between 0 and 1. The simplest form of  $\eta$  is to take  $1 - \eta$  proportional to the ice filling fraction  $f$ , but a quadratic dependence,  $\eta = (1 - f)^2$ , more closely agrees with laboratory measurements (Hudson et al., 2009). Because  $\eta$  changes little within one Mars year, it can be taken outside the time average.

Under conditions conducive to the growth of ice, the interface to a partially filled icy layer moves with time. Figure 3 illustrates the growth of ice over a short time interval. The flux through the dry layer has to supply the flux from the interface downward plus mass associated with any upward movement of the interface,

$$\bar{J}_{\text{dry}}(z_i) = \bar{J}_{\text{sat}}(z_i) - \sigma(z_i) \frac{dz_i}{dt}. \quad (6)$$

Here,  $dz_i/dt$  represents the speed of the interface, which is negative for upward movement if downward flux is positive. The use of  $\sigma(z_i)$  in this equation,

$D_{dp}$	diffusion coefficient in ice-free porous medium	(of water vapor)
$J$	vapor (mass) flux	
$T$	temperature	
$f$	fraction of pore space filled with ice	(unitless, $0 \leq f \leq 1$ for pore ice)
$t$	time	
$t_{T,eqIr}$	time for thermal model to equilibrate	(typically ten or more Mars years)
$z_g$	geothermally limited depth of pore ice	
$z_i$	depth to pore-ice/dry soil interface	
$z_{max}$	domain depth	(typically 10–20 m)
$z_t$	depth to ice sheet	
$\Delta t_B$	(big) time step for ice evolution	(typically tens to hundreds of years)
$\Delta t_T$	time step in thermal model	(typically tens of minutes)
$\Delta t_{expl.}$	time step for explicit numerical scheme	(typically a fraction of a second)
$\Phi_0$	porosity of dry soil	(unitless, typically $\Phi_0 \approx 0.4$ )
$\Phi_2$	(volumetric) ice content of ice sheet	(unitless, $\Phi_0 \leq \Phi_2 \leq 1$ )
$\eta$	constriction of vapor flux by pore ice	(unitless, $0 \leq \eta \leq 1$ )
$\rho$	water vapor density	(mass density)
$\rho_{ice}$	density of bulk ice, $\sim 927 \text{ kg/m}^3$	(mass density)
$\rho_{sv}$	saturation vapor density of $\text{H}_2\text{O}$	(mass density)
$\sigma$	density of ice relative to total volume	(mass density, $0 \leq \sigma \leq \rho_{ice}$ )

Table 1: Frequently used variables

rather than a lesser amount, is based on the assumption that the interface is infinitesimally thin even when it is moving.

Equations (3) to (6) lead to

$$\frac{\bar{\rho}_{sv}(z_i) - \bar{\rho}(0)}{z_i} = \eta(z_i) \left. \frac{\partial \bar{\rho}_{sv}}{\partial z} \right|_{z_i} + f(z_i) \frac{\Phi_0 \rho_{ice}}{D_{dp}} \frac{\Delta z_i}{\Delta t_B}. \quad (7)$$

It is convenient to define the constant

$$B = \frac{D_{dp} \Delta t_B}{\Phi_0 \rho_{ice}}. \quad (8)$$

Practically, the interface is often very close to the equilibrium depth and moves only slowly, such that the mass used to fill the volume between the interface and the equilibrium depth is much smaller than the ice mass that fills the deeper pore spaces. Hence, the rightmost term in eq. (6) is typically negligible. Even in the earliest phase of ice formation in initially dry soil, the term  $\sigma dz_i/dt$  is found to be negligible compared to  $\bar{J}_{sat}$  already after one time step.

With this approximation, the interface is located where the flux through the dry layer, eq. (3), equals

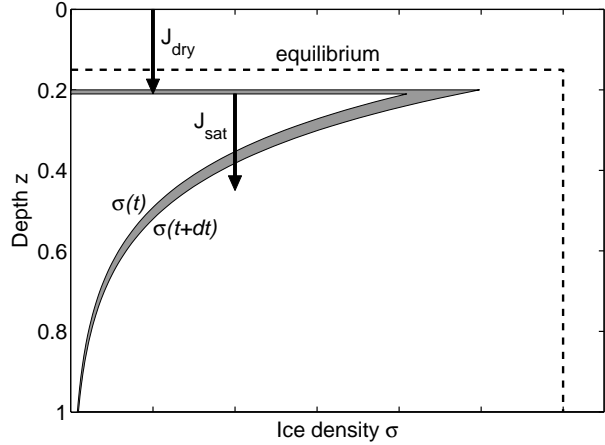


Figure 3: Illustration of ice content profile at times  $t$  and  $t+dt$  (solid lines) as well as the equilibrium profile (dash line).

the flux at the top of the icy layer, eq. (4),

$$\frac{\bar{\rho}_{sv}(z_i) - \bar{\rho}(0)}{z_i} = \eta(z_i) \left. \frac{\partial \bar{\rho}_{sv}}{\partial z} \right|_{z_i}. \quad (9)$$

Equation (9) determines the depth of the interface  $z_i$ . When pore spaces are completely filled with ice,  $\eta = 0$ , the equation reduces to the equilibrium condition  $\bar{\rho}_{sv}(z_i) = \bar{\rho}(0)$ , and the flux vanishes. When ice is stable but the pores are free of ice,  $\eta = 1$ , the interface is deeper than the equilibrium depth, and the flux is inward.

Equation (9) is solved numerically for  $z_i$ . This is done by computing the time averaged saturation vapor densities at every grid point  $\bar{\rho}_{sv}(z)$ , the time averaged vapor density on the surface  $\bar{\rho}(0)$ , numerical differentiation of the right-hand side in eq. (9), evaluation of the equality from the surface downward until the balance reverses, and linear interpolation in the spatial interval that brackets the root.

Figure 4 illustrates the equilibrium depth  $z_{eq}$ , interface depth  $z_i$ , and the lower boundary  $z_g$  due to geothermal heat discussed below. All of these three depths change with ice content. The equilibrium depth  $z_{eq}$  is not actively used in the calculation and is only diagnostic. The ultimate equilibrium depth is different from the equilibrium depth for a given ice content.

## 2.2. Rate of pore ice accumulation

Below the interface, the growth of ice within partially filled pores is governed by eq. (4) and the equation for local mass conservation,

$$\frac{\partial \sigma}{\partial t} + \frac{\partial \bar{J}_{sat}}{\partial z} = 0. \quad (10)$$

Combined with eq. (5),

$$\frac{\partial \sigma}{\partial t} = \frac{\partial}{\partial z} \left( \eta D_{dp} \frac{\partial \bar{\rho}_{sv}}{\partial z} \right). \quad (11)$$

Simple forward time differencing yields

$$\sigma^{(n+1)} = \sigma^{(n)} + \left. \frac{\partial \sigma}{\partial t} \right|^{(n)} \Delta t_B \quad (12)$$

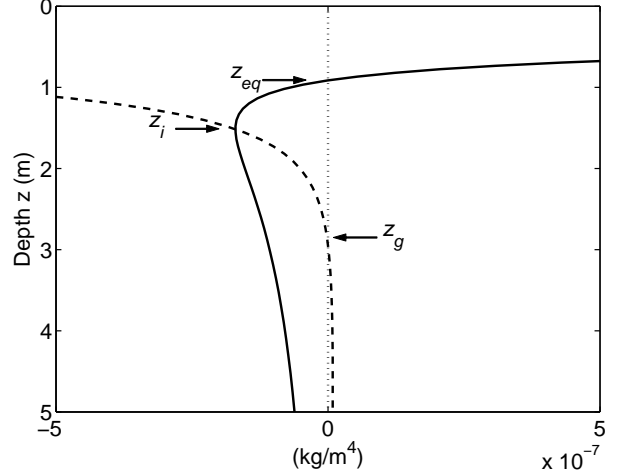


Figure 4: Vertical profiles of  $\partial \bar{\rho}_{sv}/\partial z$  (dash line) and  $(\bar{\rho}_{sv}(z) - \bar{\rho}(0))/z$  (solid line) from realistic Mars subsurface temperatures at 60°N. Three special depths are marked:  $z_{eq}$  the (instantaneous) equilibrium depth,  $z_i$  interface depth, and  $z_g$  geothermally caused bottom. In this example, ice is stable but the soil is ice-free. All three of these depths migrate with changing ice content.

or in terms of  $f$ ,

$$f^{(n+1)} = f^{(n)} + B \left. \frac{\partial}{\partial z} \left( \eta \frac{\partial \bar{\rho}_{sv}}{\partial z} \right) \right|^{(n)}. \quad (13)$$

An upper index in parentheses refers to the time step.

The temperature dependence of  $D_{dp}$  is small compared to the exponential temperature dependence of  $\rho_{sv}$ . This justifies moving  $D_{dp}$  outside of the derivative in eq. (11). Technically, only the correlation between the gradient of  $D_{dp}$  and the gradient of  $\rho_{sv}$  needs to be neglected. The equation then uses the time-averaged value of  $D_{dp}$ , which is further approximated by  $D_{dp}$  at average temperature.

The evaluation of the spatial derivatives requires special treatment, because  $\eta$  is discontinuous at the interface. This problem is solved by using a one-sided derivative for the first grid-point below an interface. Equation (11) becomes

$$\frac{\partial \sigma}{\partial t} = D_{dp} \left( \frac{\partial \eta}{\partial z} \frac{\partial \bar{\rho}_{sv}}{\partial z} + \eta \frac{\partial^2 \bar{\rho}_{sv}}{\partial z^2} \right). \quad (14)$$

A finite-difference approximation for  $\partial \eta / \partial z$  near a jump discontinuity is sought.

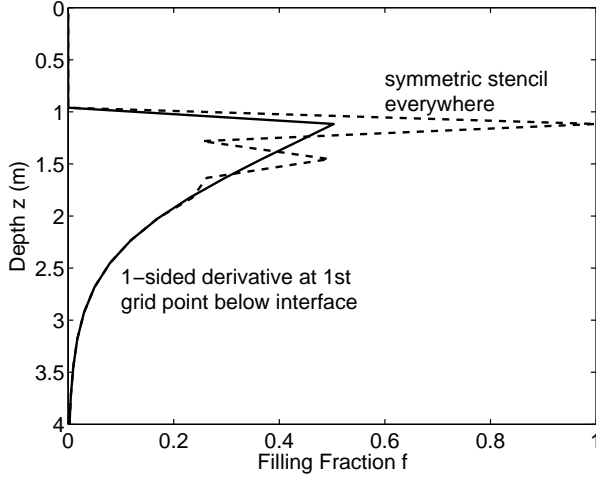


Figure 5: Comparison between the ice profile obtained with a symmetric stencil (dash line) and with the one-sided derivative at the uppermost grid point with pore ice (solid line).

A one-sided finite-difference expression for the first derivative on an irregularly spaced grid is of the form

$$\eta'(z_i) = c_1\eta(z_i + \zeta) + c_2\eta(z_i + \zeta + h_1) + c_3\eta(z_i + \zeta + h_1 + h_2) + O(\zeta^2, h_1^2, h_2^2) \quad (15)$$

where  $\zeta$  is the distance of the first grid point below the interface to the interface;  $h_1$  is the separation between the first and second grid point below the interface, and  $h_2$  that between the second and third grid point. With Taylor expansions to third order and after solving the resulting linear system of equations for the coefficients, one arrives at

$$\begin{aligned} c_1 &= -\frac{2(\zeta + h_1) + h_2}{h_1(h_1 + h_2)} \\ c_2 &= \frac{2\zeta + h_1 + h_2}{h_1h_2} \\ c_3 &= -\frac{2\zeta + h_1}{h_2(h_1 + h_2)}. \end{aligned} \quad (16)$$

Figure 5 shows a comparison between the ice profile obtained with a symmetric stencil (dash line) and with the one-sided derivative used only for the uppermost grid point below the interface (the “outermost” corner point in the displayed profile) (solid line). The

symmetric stencil leads to a numerical instability; the one-sided derivative heals the instability.

For the purpose of discussion, it is noted that eq. (14) can have an asymptotic solution that obeys

$$\frac{\partial\eta}{\partial z} \frac{\partial\bar{\rho}_{sv}}{\partial z} + \eta \frac{\partial^2\bar{\rho}_{sv}}{\partial z^2} = 0. \quad (17)$$

Typically,  $\partial\eta/\partial z > 0$ ,  $\partial\bar{\rho}_{sv}/\partial z < 0$ , and  $\partial^2\bar{\rho}_{sv}/\partial z^2 > 0$ , such that this equality could indeed be satisfied. The solution would then be of the form

$$\frac{1}{\eta} \propto \frac{\partial\bar{\rho}_{sv}}{\partial z}. \quad (18)$$

The widening pore space would compensate for the decrease in the gradient of the vapor pressure, such that the flux remains constant with depth and no deposition or loss occurs. However, an impermeable bottom boundary does not permit such a flux and a carefully implemented solver should not evolve toward such a solution.

### 2.3. A first model calculation

This concludes the discussion of the treatment of pore ice growth for an impermeable lower boundary. The lower boundary condition is

$$\frac{\partial\bar{\rho}_{sv}}{\partial z}(z_{\max}) = 0. \quad (19)$$

The impermeable lower boundary can readily be replaced with an impermeable ice sheet,

$$\frac{\partial\bar{\rho}_{sv}}{\partial z}(z_t) = 0. \quad (20)$$

A geothermal lower boundary condition will be discussed subsequently.

Figure 6 shows an example of interstitial ice growth. The reference profile involves time variable thermal properties, variable constriction, and geothermal heat. The reference profile is reliable in the sense that calculations with twice the spatial resolution or half the time step produced almost identical results.

The change in thermal properties of the ice-laden regolith is important quantitatively. Two parametrizations of thermal properties for ice-laden

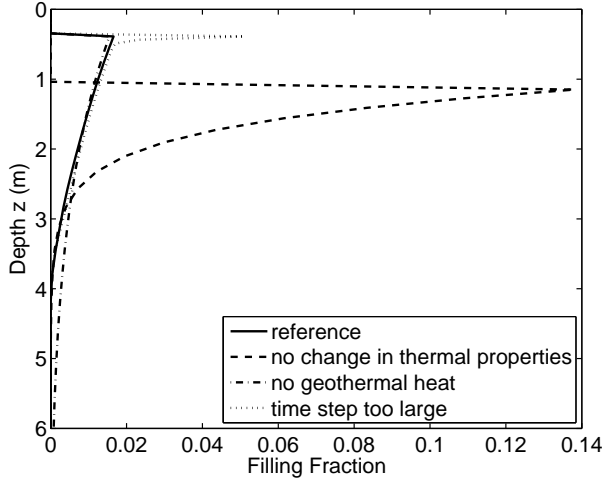


Figure 6: Growth of pore ice after 10 ka starting with initially ice-free regolith. A synthetic sinusoidal temperature oscillation is applied on the surface with a mean of 192 K and an amplitude of 20 K. Other parameters are:  $\Phi_0 = 0.4$ ,  $D_{\text{dp}} = 4 \times 10^{-4} \text{ m}^2 \text{ s}^{-1}$ , and  $\Delta t_B = 25 \text{ yr}$ . The partial pressure of  $\text{H}_2\text{O}$  on the surface is 0.2 Pa.

soil were used in example calculations. One is a simple linear combination of the properties of dry soil and ice (Schorghofer and Aharonson, 2005) and the other a nonlinear model proposed by Mellon et al. (1997).

#### 2.4. Geothermal heat at lower boundary

Geothermal heat leads to an increase in temperature with depth, which can drive vapor upward, and may limit the maximum depth of stability for an ice layer. This problem has been investigated by Hudson (2008), and is here developed independently. The bottom is assumed to be impermeable and there is no supply of vapor from below.

First, we consider the physics beneath the bottom end of a pore ice layer, which by definition is ice-free. A geothermal temperature profile linearly increasing with depth causes  $\partial \bar{\rho}_{sv} / \partial z$  to be positive, driving vapor upward (4). For the same linear temperature profile,  $\partial^2 \bar{\rho}_{sv} / \partial z^2$  is still positive and would thus imply accumulation of ice (11). However, if no ice is present, the vapor density is no longer given by  $\bar{\rho}_{sv}$ , as implicitly assumed in eqs. (4) and (11). This

explains why the equation for ice accumulation is invalid over this range of depths. With the flux upward and no source of ice beneath, the accumulation rate must vanish,  $\partial \sigma / \partial t = 0$ . Hence, if  $\sigma$  is zero initially, it can be always set to zero where the flux is upward. The depth of the bottom boundary  $z_g$  is given by the depth of flux reversal,

$$\left. \frac{\partial \bar{\rho}_{sv}}{\partial z} \right|_{z_g} = 0, \quad (21)$$

if there is no ice beneath this depth.

A more general situation needs to be considered. Temperature profiles can change as a result of changing soil conductivity and surface heat budget. The net flux can change from downward to upward with pores containing ice. Equation (21) is no longer applicable if the ice beneath the current value of  $z_g$  lasts for more than one time step.

The equation for movement of the lower boundary is determined by  $\text{H}_2\text{O}$  mass conservation. The mass lost by the receding bottom ice boundary equals the upward flux at the boundary,

$$\rho_{\text{ice}} f(z_g) \Phi_0 \frac{dz_g}{dt} = \eta D_{\text{dp}} \left. \frac{\partial \bar{\rho}_{sv}}{\partial z} \right|_{z_g}. \quad (22)$$

If no ice is present at depth  $z_g$ ,  $f(z_g) = 0$ , then the boundary resides where the flux reverses, eq. (21). To some approximation,

$$\rho_{\text{ice}} \Phi_0 \int_{z_g(0)}^{z_g(\Delta t_B)} \frac{f(z)}{\eta(z)} dz = D_{\text{dp}} \left. \frac{\partial \bar{\rho}_{sv}}{\partial z} \right|_{z_g} \Delta t_B. \quad (23)$$

The right-hand side of this expression is positive when the flux is upward. Because the left-hand side is always positive, the integral should never go further than the sign reversal on the right-hand side. Hence, the lower boundary of the ice cannot be shallower than the  $z_g$  determined from eq. (21). The lower integration boundary can be replaced with the domain depth  $z_{\text{max}}$ . Thus,

$$\int_{z_{\text{max}}}^{z_g(\Delta t_B)} \frac{f(z)}{\eta(z)} dz = B \left. \frac{\partial \bar{\rho}_{sv}}{\partial z} \right|_{z_g} \quad (24)$$

where  $B$  happens to be the same as in eq. (8). This procedure reduces to eq. (21) when no ice is present. It is only applied where the flux is upward.

In the case  $\eta = 0$ , the ice layer is impermeable and, if the flux is upward,  $z_g$  does not move at all.

### 3. Retreat of Ice

As ice is lost to the atmosphere, two cases are distinguished, as shown in Figure 2. One is an ice sheet that consists of ice, including excess ice, and regolith or dust that stays behind as the ice retreats. It does not accommodate any void space (air) below the ice table. This case is treated in section 3.1, and a layer of pure ice is a special case thereof. The other, treated in section 3.2, is a layer of interstitial ice, where the pores are partially or fully filled with ice, but no excess ice is present, such that the soil matrix remains the same as the ice retreats.

#### 3.1. Retreat of ice sheet

Here we consider the retreat of pure ice and of dirty ice that leaves a sublimation lag. The vapor flux from the ice to the atmosphere is given by

$$\bar{J} = -D_{\text{dp}} \frac{\bar{\rho}_{sv}(z_t) - \bar{\rho}(0)}{z_t}, \quad (25)$$

where  $z_t$  is the depth of the ice table (the thickness of the dry layer), and  $\bar{\rho}(0)$  the vapor density on the surface.

The rate of retreat of a pure ice layer is

$$r = -\bar{J}/\rho_{\text{ice}}, \quad (26)$$

where  $\rho_{\text{ice}}$  is the density of bulk ice,  $\sim 927 \text{ kg/m}^3$ . For an ice sheet that contains soil, several geometric factors need to be introduced. On average, an areal fraction of  $1 - \Phi_2$  of the ice table surface is not ice, but the flux is limited by how much can pass through the dry layer not by how much is supplied; irrespective of  $\Phi_2$ , there is a saturated layer of vapor above the ice table. Thus the flux is still given by eq. (25). The dirty ice retreats at a rate of

$$r_m = -\frac{\bar{J}}{\Phi_2 \rho_{\text{ice}}} = \frac{r}{\Phi_2}, \quad (27)$$

faster than pure ice, eq. (26).

As the ice table retreats, any soil contained in the ice transitions to the layer of dry soil. The relation between the rate of ice retreat,  $r_m$ , and the rate at which the dry layer grows,  $dz_t/dt$ , is determined by the balance of soil mass:

$$(1 - \Phi_2)r_m = (1 - \Phi_0) \frac{dz_t}{dt}. \quad (28)$$

Hence, the dry layer grows at a rate

$$\frac{dz_t}{dt} = \frac{1 - \Phi_2}{1 - \Phi_0} \frac{1}{\Phi_2} r. \quad (29)$$

The geometric prefactor can be collected into a single constant

$$\beta = \frac{1 - \Phi_2}{1 - \Phi_0} \frac{1}{\Phi_2}, \quad (30)$$

such that

$$\frac{dz_t}{dt} = \frac{\beta D_{\text{dp}} \bar{\rho}_{sv}(z_t) - \bar{\rho}(0)}{\rho_{\text{ice}} z_t}. \quad (31)$$

For brevity we define  $\Delta\bar{\rho} = \bar{\rho}_{sv}(z_t) - \bar{\rho}(0)$ . This would lead to a forward time-difference of

$$z_t(\Delta t_B) = z_t(0) + \beta \frac{D_{\text{dp}} \Delta\bar{\rho}}{z_t \rho_{\text{ice}}} \Delta t_B, \quad (32)$$

but this expression can be readily improved.

Both,  $\Delta\bar{\rho}$  and  $z_t$  in eq. (31) vary with time. We can at least account for the change in  $z_t$  over one time step with a simple integration of eq. (31) from 0 to  $\Delta t_B$ ,

$$z_t^2(\Delta t_B) - z_t^2(0) = 2\beta D_{\text{dp}} \frac{\Delta\bar{\rho}}{\rho_{\text{ice}}} \Delta t_B. \quad (33)$$

Out of necessity,  $\Delta\bar{\rho}$  is evaluated at the beginning of the time step, and the advance will be too large when  $\Delta\bar{\rho}$  decreases rapidly with depth, as is the case when the ice is very shallow. Nevertheless, eq. (33) is an improvement over a simple forward time-difference, eq. (32), and leads to

$$z_t^{(n+1)} = \sqrt{z_t^{(n)2} + 2D_{\text{dp}}\beta \frac{\Delta\bar{\rho}^{(n)}}{\rho_{\text{ice}}} \Delta t_B}. \quad (34)$$

For one particular initial configuration, when ice reaches to the surface, eq. (31) breaks down because

$z_t = 0$ . Physically, the retreat rate is still limited by convection of water vapor into the atmosphere. Equation (34) involves a thickening of the sublimation till over a single time step and thus happens to heal the divergence. Practically, there is a worse problem for this initial configuration caused by the fact that  $\bar{\rho}_{sv}$  is extremely large on the surface and decays so rapidly with depth that only a small time step is permissible, otherwise the ice table advances too far. Hence, an initial ice sheet that reaches to the very surface is taken care of with a model spin-up, with time steps that begin at near zero and then increase geometrically.

### 3.2. Retreat of interstitial ice

Interstitial ice is lost from the interface to the atmosphere, while ice may simultaneously grow below the interface.

The retreat of pore ice can be handled similarly to the retreat of an ice sheet. The flux is again given by eq. (25). The retreat rate is

$$r_p = -\frac{\bar{J}}{f\Phi_0\rho_{\text{ice}}} = \frac{r}{f\Phi_0}. \quad (35)$$

The depth  $z_t$  is replaced by the shallowest depth with perennial ice  $z_p$  and  $dz_p/dt = r_p$  instead of eq. (29). Note that  $z_p$  does not necessarily have to coincide with  $z_i$ , because climate conditions may change so rapidly that the ice does not retreat fast enough to follow  $z_i$  as defined by eq. (9). Usually,  $z_p$  and  $z_i$  do coincide.

Integration now yields,

$$\int_{z_p(0)}^{z_p(\Delta t_B)} f(z)z dz = \int_0^{\Delta t_B} \frac{1}{\Phi_0} \frac{D_{\text{dp}}}{\rho_{\text{ice}}} \Delta\bar{\rho} dt. \quad (36)$$

By definition there is no ice above  $z_p(0)$ , and thus the lower integration boundary on the left-hand side may as well be set to zero. The left-hand side is integrated numerically to determine  $z_p(\Delta t_B)$ . As above,  $\Delta\bar{\rho}$  is evaluated at the beginning of the time step, and the integration on the right-hand side thus reduces to multiplication with  $\Delta t_B$ . Using again the constant  $B$ , eq. (36) becomes,

$$\int_0^{z_p(\Delta t_B)} f(z)z dz = B\Delta\bar{\rho}(z_p(0)). \quad (37)$$

In different notation,

$$\int_0^{z_p^{(n+1)}} f^{(n)}z dz = B\Delta\bar{\rho}^{(n)}(z_p^{(n)}), \quad (38)$$

which is solved numerically for  $z_p^{(n+1)}$ .

The maximum retreat is limited by the interface depth calculated from eq. (9), and eq. (37) only becomes effective when the retreat is slower than the downward movement of the interface depth. Otherwise, all ice above the newly calculated interface depth disappears.

## 4. Overall Scheme

The retreat of an ice sheet, the retreat of pore ice, and the growth of pore ice form a closed set of processes for the evolution of subsurface ice. An ice sheet, that may have formed from precipitated snow or ice, enters calculation only as initial condition, or would otherwise have to be added as an additional process. Conditional statements decide which of these three processes is taking place at any given time and location.

### 4.1. Time sequencing

At every time step, the model first runs a thermal calculation until temperatures have equilibrated. Annual averages are calculated from the last Mars year. The annual means are then used to advance the interface by a (big) time step  $\Delta t_B$  and grow pore ice where stable. In the next time step, the thermal model is rerun, and so on. The thermal properties of the soil are updated at every time step.

At each step, the thermal model needs to be run for a number of Mars years until temperatures equilibrate. Averages are taken from the last Mars year. The length of this equilibration time  $t_{\text{T,eq}}$  will depend on the depth of the domain and the quality of the initial temperature guess. For a domain depth of 20 m, 15 Mars years are often found to be sufficient.

The part of the temperature profile that adjusts the slowest is the bottom temperature. At the very beginning of the model run, the temperature profile is equilibrated for a long period, e.g. 100 Mars years.

Subsequently, a time  $t_{T,\text{eq}}^{\text{lr}}$  is used for equilibration, but the bottom temperature of the previous time step is passed for initialization.

The ice growth is calculated over a time step  $\Delta t_B$ . The maximum time step allowed turns out to depend on how sensitive the thermal properties of the subsurface depend on ice content. Without any such dependence, steps of hundreds of years are readily possible. With thermal conductivity changes, especially when the thermal conductivity involves a square root dependence on ice content, as it does for the parametrization of Mellon et al. (1997), steps as small as a few years are required, otherwise the ice content near the interface may be unreliable (Figure 6). If desired, the time step can be chosen arbitrarily short, but seasonal and diurnal exchange are never reproduced.

Actual (physical) time evolves in steps of  $\Delta t_B$ . The thermal evolution over  $t_{T,\text{eq}}^{\text{lr}}$  may be considered virtual time, because no update of soil or external conditions takes place. When output is desired every 1,000 (Earth) years, then  $\Delta t_B$  should be an integer fraction of 1 ka.

#### 4.2. Estimate of speed-up

By design, the climate model uses asynchronous coupling; the time step for the thermal model is a fraction of an hour while that for the ice evolution is many Mars years. Nevertheless, it would be possible to evolve the model synchronously in the sense of  $\Delta t_B = t_{T,\text{eq}}^{\text{lr}} = 1$  or asynchronously,  $\Delta t_B \neq t_{T,\text{eq}}^{\text{lr}}$ .

In terms of speed the synchronous choice turns out to be less efficient, as will become clear from the following discussion. Additional speedup can be achieved with additional asynchronous coupling.

The averaging of the vapor pressure involves exponential functions, which are slower than floating-point operations typically by a factor of 10 to 40. Hence, we distinguish between the time necessary to execute a floating-point operation,  $\delta_{\text{fp}}$ , and the time to evaluate an exponential function,  $\delta_{\text{ex}}$ .

In the introduction it was estimated that the speedup of the fast method compared to an explicit model is  $\Delta t_T / \Delta t_{\text{expl.}} \sim 10^4$ . A more detailed estimate is obtained here. The number of simulated

Mars years per second of computation time is proportional to a speed factor  $S$ , which is estimated for the various models as follows. For the implicit or semi-implicit thermal model,

$$S_T = \frac{\Delta t_T}{\delta_{\text{fp}}}. \quad (39)$$

Explicit vapor diffusion and deposition model,

$$S_{\text{expl.}} = \frac{\Delta t_{\text{expl.}}}{\delta_{\text{ex}} + \delta_{\text{fp}}}. \quad (40)$$

Fast vapor deposition model

$$S_{\text{fast}}^{(\text{syn})} = \frac{\Delta t_T}{\delta_{\text{fp}} + \delta_{\text{ex}}} \quad (\text{synchronous}) \quad (41)$$

$$S_{\text{fast}}^{(\text{asyn})} = \frac{\Delta t_B \Delta t_T}{t_{T,\text{eq}}^{\text{lr}} \delta_{\text{fp}} + \delta_{\text{ex}}} \quad (\text{asynchronous}) \quad (42)$$

where  $t_{T,\text{eq}}^{\text{lr}}$  is in units of Mars years.

Expression (42) reveals that the thermal equilibration time  $t_{T,\text{eq}}^{\text{lr}}$  is not the dominant cost unless it is longer than  $\delta_{\text{ex}} / \delta_{\text{fp}}$ , that is, 10 to 40 Mars years, because evaluation of the vapor pressure in the last Mars year dominates the cost.

The estimated speedup compared to an explicit vapor diffusion model is

$$\frac{S_{\text{fast}}^{(\text{syn})}}{S_{\text{expl.}}} = \frac{\Delta t_T}{\Delta t_{\text{expl.}}} \approx \frac{10^3}{0.1} = 10^4. \quad (43)$$

This confirms the naive guess for the expected speedup given in the introduction. The fast synchronous method is about four orders of magnitudes faster than an explicit vapor deposition model. The factor is gained due to the relaxation of the time step requirement, by switching from microphysical equations to the equations for net mass balance.

Let  $s = \delta_{\text{ex}} / \delta_{\text{fp}} \approx 20$ , then

$$\frac{S_{\text{fast}}^{(\text{asyn})}}{S_{\text{expl.}}} \approx \frac{\Delta t_T}{\Delta t_{\text{expl.}}} \Delta t_B \frac{1 + s}{t_{T,\text{eq}}^{\text{lr}} + s} \quad (44)$$

$$\approx \frac{10^3}{0.1} \times 25 \times \frac{1 + 20}{10 + 20} \approx 10^5. \quad (45)$$

Hence the fast method is about five orders of magnitudes faster than an explicit vapor deposition model.

The additional speedup is due to the asynchronous coupling,

$$\frac{S_{\text{fast}}^{(\text{asyn})}}{S_{\text{fast}}^{(\text{syn})}} = \Delta t_B \frac{1+s}{t_{T,\text{eq}} + s} \approx 25 \times \frac{1+20}{10+20} \approx 18. \quad (46)$$

Also of interest is the speed compared to (the subsurface component of) a purely thermal model

$$\frac{S_{\text{fast}}^{(\text{syn})}}{S_T} = \frac{1}{1+s} \approx \frac{1}{1+20} \approx 0.05. \quad (47)$$

Hence the synchronous fast method is about one order of magnitude slower than a thermal model. This remaining tardiness is due to the evaluation of exponentials for the vapor pressure. Use of the asynchronous method happens to make up for that,

$$\frac{S_{\text{fast}}^{(\text{asyn})}}{S_T} = \frac{\Delta t_B}{t_{T,\text{eq}} + s} \approx \frac{25}{10+20} \approx 1. \quad (48)$$

Hence, the ice evolution can be computed as fast as temperatures.

#### 4.3. Implementation

The accelerated numerical method has been implemented in Fortran 95, and the source code is available online for use by the scientific community. It is the asynchronous version of the model that has been implemented. A great number of conditional statements is used to switch among different processes at different depths and among the two situations in Figure 2.

The programs and subroutines were developed in three major cycles, on top of the thermal model that is common to all of them. These development cycles can still be recognized in the organization of program units. The first development cycle achieved the growth of pore ice, without the possibility for retreat and without an ice sheet. The second cycle included the retreat of ice but still uses synthetic surface temperatures, such as a sinusoidal time dependence. The third cycle then uses insolation driven temperatures with actual Mars orbit. Compared to the synthetic temperatures, many additional variables need to be passed to the subroutines.

When the model is applied not only to a single site, but to many sites simultaneously, such as a grid

spanning the entire globe, the size of the output files should remain manageable. Depth profiles of temperature and water vapor density do not need to be stored, but the depth profile of ice content is needed. The file size can be reduced by avoiding trailing zeros wherever the ice content is zero.

#### 4.4. The M-SIM (Mars Subsurface Ice Model) program collection

A collection of subroutines and driving programs is made available on the web, including the numerically accelerated model described here. They are currently available from the author's website at [www2.hawaii.edu/~norbert/m-sim/](http://www2.hawaii.edu/~norbert/m-sim/). Although many of these implementations and the numerical methods underlying them could be improved, these functional components are intended to facilitate modeling for the research community.

At this point in time, M-SIM includes the following model components:

1. Semi-implicit thermal model
2. Explicit vapor diffusion and deposition model
3. Equilibrium models of the ice table
4. Fast method of ice growth and retreat

Part 4 is described in the present article. Part 3 is used extensively in Schorghofer and Aharonson (2005) and Aharonson and Schorghofer (2006). Part 2 has been described in appendix B of Schorghofer and Aharonson (2005), and part 1 is described in technical notes also available on the M-SIM website. All the models are essentially one-dimensional, but the surface energy balance of horizontal and sloped surfaces can be coupled.

## 5. Two Applications

The capabilities of the fast model are best illustrated with two specific examples. Both involve time integration over hundreds of thousands of years, time periods that are inaccessible with conventional models. The effective speed was roughly 100,000 years of simulation per one hour of computation time, on a new workstation.

Beyond of what has been described above, these model simulations include varying orbital elements based on Laskar et al. (2004) and require assumptions about the history of atmospheric humidity. The last precipitation dates from a different obliquity epoch (Head et al., 2003; Mischna et al., 2003; Levrard et al., 2004; Forget et al., 2006). It is not reliably known when the last ice sheet formed by precipitation or how humidity varied with time. An obliquity near  $\sim 47^\circ$  was last reached about 5640 ka ago; and an obliquity of  $\sim 35^\circ$  has not been exceeded since 632 ka ago.

Two extreme humidity scenarios are considered. One where the partial pressure of  $\text{H}_2\text{O}$  does not vary at all from year to year, and only the temperature changes due to the orbital variations. The other extreme is a humidity purely controlled by sublimation loss from the North Polar cap (Toon et al., 1980), without any limitations for the vapor transport from the poles to lower latitudes. Realistic humidity histories lie between these two extremes. The atmospheric humidity for this variable humidity scenario depends mainly on obliquity and to a lesser degree on eccentricity and the longitude of Mars' perihelion.

The model uses a constant atmospheric pressure, and thus the duration and extent of the seasonal  $\text{CO}_2$  cover does not change with orbital configuration, which is somewhat unrealistic. The number of numerical grid points is 80–110, with six points residing within the diurnal skin depth.

### 5.1. Ice near the geographic permafrost margin

The Gamma Ray and Neutron Spectrometer onboard Mars Odyssey found a high abundance of the element hydrogen poleward of roughly  $60^\circ$  latitude on both hemispheres (Boynton et al., 2002; Feldman et al., 2002; Mitrofanov et al., 2002; Feldman et al., 2004). Both, equilibrium and non-equilibrium models, predict that the margin (latitudinal boundary) of the two hemispheric ice layers moved over the past few million years (Mellon and Jakosky, 1993, 1995; Schorghofer, 2007a).

The subsurface model simulates the growth of ice in interstitial soil pores from atmospherically derived water vapor and the retreat of pore ice. The simulations begin arbitrarily 1 Ma ago. The present margins

are assumed to have been depleted at least once since the last precipitation, and thus there is no initial ice sheet. The bottom boundary of the subsurface ice is restricted by a geothermal heat flux of  $28 \text{ mW/m}^2$ . Figure 7 shows results for a latitude of  $55^\circ\text{N}$ .

Figure 7a and 7b show burial depths and the lower boundary of the ice for the two humidity histories. Retreats coincide with periods of low obliquity; at this particular latitude, annual mean temperature is high when obliquity is low and vice versa (Schorghofer, 2008b). The difference between the geothermally limited depth of the ice and the depth of the ice table is the thickness of the ice-rich layer. At  $55^\circ\text{N}$ , the ice becomes repeatedly unstable and its thickness is limited by the time available for growth; it never reaches more than several meters.

Figure 7c shows the ice content for both humidity scenarios. The thickness is a few meters and the pores are only partially filled with ice.

Figure 7d shows the column integrated amounts of ice. The result strongly depends on the humidity history, but in both cases depletion proceeds faster than recharge. This is physically plausible, because the retreat rate is limited by diffusion but the recharge rate is limited not only by diffusion but also by the ability to pump vapor downward. Hence, two different time scales are involved.

Subsurface ice retreats rapidly when it is unstable near the geographic margins and the volume changes are significant. It is plausible that the layers of the Polar Deposits are the result of contractions of the ice-rich permafrost.

### 5.2. History of ice at the Phoenix landing site

The Phoenix Lander touched down at  $68.2^\circ\text{N}$  and verified the existence of water ice beneath the dry surface (Smith et al., 2009; Mellon et al., 2009; Sizemore et al., 2010). Equilibrium models indicate that the depth of the ice table is indeed consistent with atmosphere-subsurface exchange (Mellon et al., 2009). Model calculations of the ice history using an older and less developed implementation of the fast method were described in Schorghofer (2008a), prior to landing. These calculations predicted that nearest the surface is interstitial pore ice instead of an ice sheet and that the pores should be completely

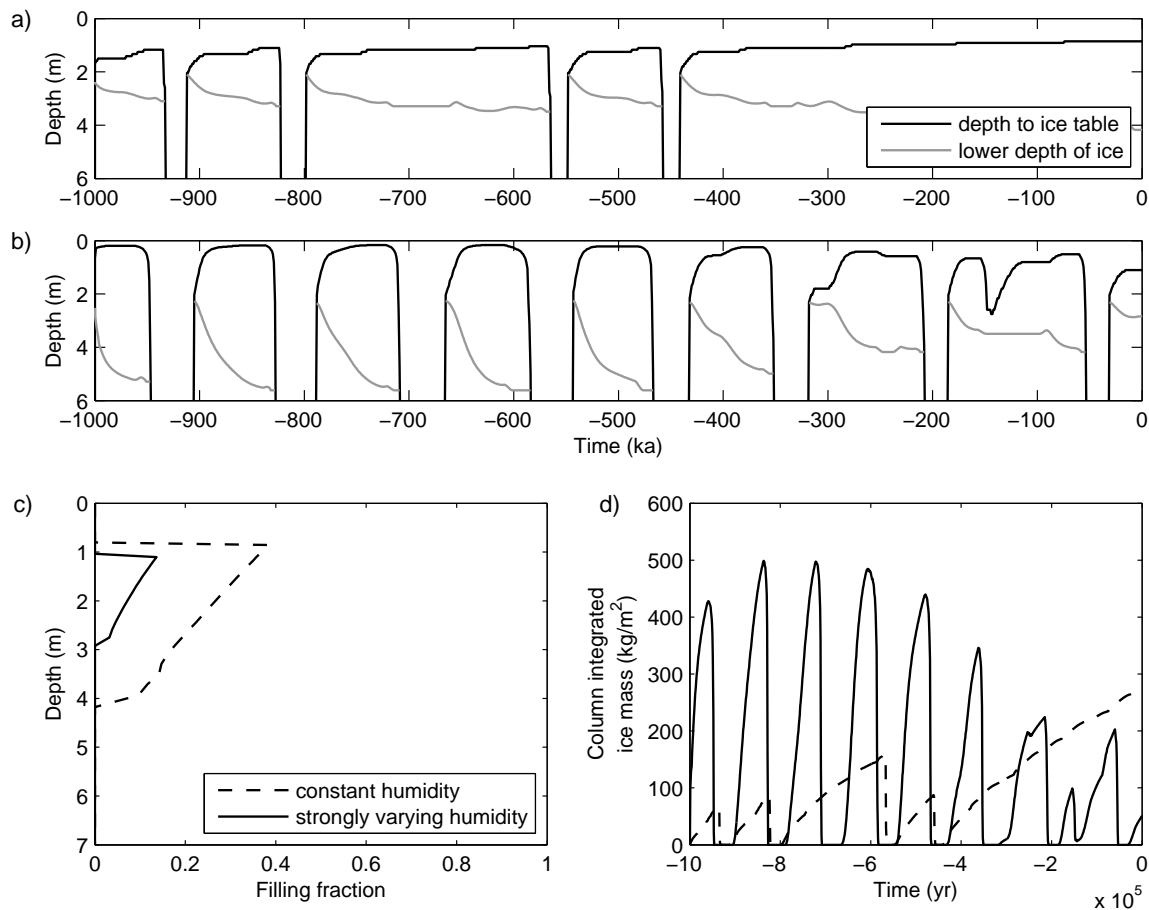


Figure 7: Retreat and growth of pore ice in a model study for  $55^\circ\text{N}$  latitude from 1 Ma ago to the present. a) Ice depths when the atmospheric humidity is constant with time. b) Ice depths when atmospheric humidity varies strongly with orbital configuration. c) Present-day vertical distribution of water ice for both humidity scenarios. d) Time history of the column integrated ice mass for the two climate scenarios. Depletion proceeds faster than recharge. Model parameters:  $\Phi_0 = 0.4$ ,  $\Delta t_B = 50$  years,  $\Delta t_T = 0.02$  sols.

filled with ice. These conclusions are confirmed by the more definite simulations described in the following.

To determine the vertical distribution and age of ground ice, it is necessary to consider the history of the ice since the last precipitation. The model of the evolution of subsurface ice layers is applied to the landing site. Various assumed parameters are listed in Table 2. The initial ice sheet is 20 m thick, but the behavior in the upper meter of the surface depends

little on the total sheet thickness.

Figure 8 shows the time variation of ice table depths for a climate scenario where the last ice sheet formed 632 ka ago at an obliquity of  $\sim 35^\circ$ . The upper interface is that between ice-free soil and pore ice. The lower ice table is the top of the almost pure ice sheet. During dry or warm periods, interstitial pore ice recedes, and after all pore ice is lost, the ice sheet retreats to greater depth. During humid or cold periods, pore ice forms, while the ice sheet remains at

latitude	68.2°N
albedo	0.2
thermal inertia of dry soil	250 <sup>†</sup>
thermal inertia of icy soil	250–1826 <sup>†</sup>
thermal inertia of ice sheet	2176 <sup>†</sup>
porosity of dry soil	50%
dust content of ice sheet	5%
density of dry soil	1608 kg m <sup>-3</sup>
heat capacity of dry soil	800 J kg <sup>-1</sup> K <sup>-1</sup>
atmospheric pressure	784 Pa
atmospheric absorption	4% in zenith
atmospheric scattering	2% in zenith
thermal model time step $\Delta t_T$	0.02 sols
ice model time step $\Delta t_B$	200 yr
equilibration time $t_{T,eqlr}$	10 Mars yr

Table 2: Model parameters for the Phoenix landing site study.  
<sup>†</sup> unit is J m<sup>-2</sup>K<sup>-1</sup>s<sup>- $\frac{1}{2}$</sup>

constant depth. In both scenarios the pore ice depth has barely changed in the past 25 ka.

Figure 9 shows the model results for the vertical ice profile. The pores are completely full in the pore ice layer. Deposition was sufficiently fast to lead to such high ice content. Time progression of the vertical ice profiles reveals that the pore ice interface grows upward with essentially full pores below the interface. For the second humidity scenario, the ice profile (not shown) also has essentially completely full pores.

For a prescribed atmospheric partial pressure of 0.2 Pa, the annual mean molecular number densities on the surface varied between  $1.2 \times 10^{19}$  and  $2.1 \times 10^{19}$  molecules m<sup>-3</sup>, with a present-day value of  $1.8 \times 10^{19}$ . For the variable humidity scenario this density varies between zero and over  $10^{20}$  molecules m<sup>-3</sup>.

For both climate scenarios considered here, the following is true: (i) Nearest the surface is interstitial pore ice instead of an almost pure ice sheet (Schorghofer, 2007a), and (ii) The pore filling fraction is close to its maximum. Both are consistent with observations by the Phoenix Lander (Mellon et al., 2009), where most of the ice was found to be pore ice with some patches of almost pure ice.

If the last precipitation occurred earlier than 632 ka ago, then the ice sheet lies deeper beneath the surface

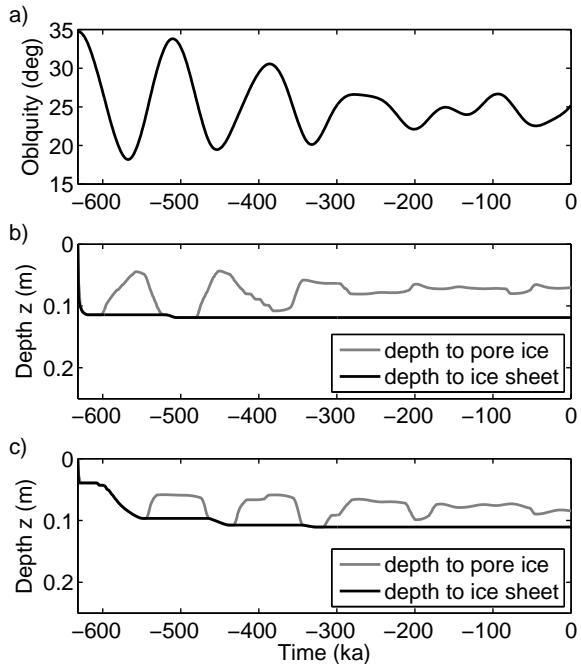


Figure 8: Retreat and growth of ice in a model study for the Phoenix Landing site. a) Tilt of rotation axis of planet. In b) the atmospheric humidity is assumed to be constant. In c) atmospheric humidity varies strongly with orbital configuration. Both scenarios lead to a three-layered depth distribution with a thin layer of pore ice.

while the depth to pore ice will be about the same.

There is an important conclusion to be drawn from a comparison of the constant humidity and strongly varying humidity scenario in Figure 8. The pore ice depths evolve out of phase. When the humidity is constant, then higher obliquity implies higher temperature and thus a retreat of pore ice. On the other hand, the supply of vapor from the North Polar cap is much higher at high obliquity, which overcompensates for the change in temperature, leading to shallower pore ice at high obliquity. A consequence of this is that an intermediate humidity scenario may have a pore ice layer thinner than either of the two extreme scenarios. Hence, the pore ice layer can be very thin.

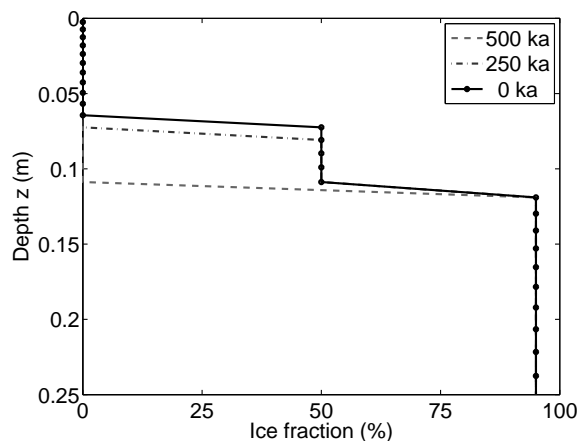


Figure 9: Three snapshots of the vertical distribution of water ice for the same simulation as in Figure 8b. Soil porosity is 50% and the ice content of the ice sheet is 95%. The interfaces are only one numerical grid point thick.

## 6. Summary

An accelerated numerical method is described for the long-term evolution of subsurface ice (much longer than one Mars year). Processes incorporated are growth of interstitial pore ice from atmospherically derived vapor, retreat of pore ice by loss to the atmosphere, retreat of an ice sheet by loss to the atmosphere, and retreat of pore ice due to geothermal heating from below.

For this purpose, we have derived equations for the depth to the pore ice interface, eq. (7), the growth rate of pore ice, eq. (13), and the lower boundary condition with and without the presence of geothermal heat, respectively eqs. (19) and (24). We also worked out retreat rates for various cases and formulas for the advance of ice tables over a time step, eqs. (34) and (38). Some of the numerical issues that had to be addressed are a one-sided derivative for the constriction function during pore ice growth and a spin-up phase when initially the ice reaches all the way to the surface.

The accelerated method is five orders of magnitude faster than explicit vapor transport calculations, eq. (45), when diurnal variations are to be resolved. Its speed matches that of purely thermal models, eq.

(48). The speedup is achieved mainly by solving the time-averaged equations for vapor transport and ice volume change. The time step is ultimately limited by how strongly the thermal properties of the ice-laden soil depend on ice content. In realistic model simulations, one hour of computation time can follow 100 ka of subsurface ice dynamics on Mars with half-hour time steps for the thermal model.

The numerical method has been implemented and applied to two problems.

Near the margins of the ice-rich permafrost at  $55^\circ$  latitude, ice is repeatedly depleted and slowly recharged, leading to a pore ice layer estimated to be currently no more than a few meters thick. The ice accumulates slowly when it is stable but retreats rapidly when it is unstable.

At the Phoenix Landing Site the model shows the growth of a three layered structure, whereby the layer of pore ice can be very thin. These calculations predicted that nearest the surface is interstitial pore ice instead of an almost pure ice sheet and that the pores should be almost completely filled with ice, in agreement with the observations (Mellon et al., 2009).

**Acknowledgments:** This material is based upon work supported by NASA under grant no. NNX09AI72G issued through the Mars Fundamental Research Program.

## References

- Aharonson, O., Schorghofer, N., 2006. Subsurface ice on Mars with rough topography. *J. Geophys. Res.* 111 (E11), E11007.
- Ames, W. F., 1992. *Numerical Methods for Partial Differential Equations* (Third ed.). Academic Press.
- Boynton, W. V., et al., 2002. Distribution of hydrogen in the near-surface of Mars: evidence for subsurface ice deposits. *Science* 297 (5578), 81–85.
- Chevrier, V., et al., 2007. Sublimation rate of ice under simulated Mars conditions and the effect of layers of mock regolith JSC Mars-1. *Geophys. Res. Lett.* 34, L02203.

- Clifford, S. M., Hillel, D., 1986. Knudsen diffusion: The effect of small pore size and low gas pressure on gaseous transport in soil. *Soil Science* 141 (4), 289.
- Feldman, W. C., et al., 2002. Global distribution of neutrons from Mars: Results from Mars Odyssey. *Science* 297 (5578), 75–78.
- Feldman, W. C., Prettyman, T. H., Maurice, S., Plaut, J. J., Bish, D. L., Vaniman, D. T., Mellon, M. T., Metzger, A. E., Squyres, S. W., Karunatillake, S., Boynton, W. V., Elphic, R. C., Funsten, H. O., Lawrence, D. J., Tokar, R. L., 2004. The global distribution of near-surface hydrogen on Mars. *J. Geophys. Res.* 109 (E09), E09006.
- Flasar, F. M., Goody, R. M., 1976. Diurnal behavior of water on Mars. *Planet. Space Sci.* 24 (2), 161–181.
- Forget, F., Haberle, R. M., Montmessin, F., Levrard, B., Head, J. W., 2006. Formation of glaciers on Mars by atmospheric precipitation at high obliquity. *Science* 311 (5759), 368–371.
- Head, J. W., Mustard, J. F., Kreslavsky, M. A., Milliken, R. E., Marchant, D. R., 2003. Recent ice ages on Mars. *Nature* 426, 797–802.
- Helbert, J., Benkhoff, J., 2003. A new approach to assessing the burial depth of ground ice deposits and its application to proposed MER landing sites in Isidis Planitia. *J. Geophys. Res.* 108 (E12), 8087.
- Hudson, T. L., 2008. *Growth, Diffusion, and Loss of Subsurface Ice on Mars: Experiments and Models*. Ph. D. thesis, Caltech, Pasadena, California.
- Hudson, T. L., Aharonson, O., 2008. Diffusion barriers at Mars surface conditions: salt crusts, particle size mixtures, and dust. *J. Geophys. Res.* 113, E09008.
- Hudson, T. L., Aharonson, O., Schorghofer, N., 2009. Laboratory experiments and models of diffusive emplacement of ground ice on Mars. *J. Geophys. Res.* 114, E01002.
- Hudson, T. L., Aharonson, O., Schorghofer, N., Farmer, C. B., Hecht, M. H., Bridges, N. T., 2007. Water vapor diffusion in Mars subsurface environments. *J. Geophys. Res.* 112 (E5), E05016.
- Jakosky, B. M., 1983. The role of seasonal reservoirs in the Mars water cycle. 1. seasonal exchange of water with the regolith. *Icarus* 55 (1), 1–18.
- Laskar, J., Correia, A. C. M., Gastineau, M., Joutel, F., Levrard, B., Robutel, P., 2004. Long term evolution and chaotic diffusion of the insolation quantities of Mars. *Icarus* 170, 343–364.
- Levrard, B., Forget, F., Montmessin, F., Laskar, J., 2004. Recent ice-rich deposits formed at high latitudes on Mars by sublimation of unstable equatorial ice during low obliquity. *Nature* 431 (7012), 1072–1075.
- Mellon, M. T., Arvidson, R. E., Sizemore, H. G., Searls, M. L., Blaney, D. L., Cull, S., Hecht, M. H., Heet, T. L., Keller, H. U., Lemmon, M. T., Markiewicz, W. J., Ming, D. W., Morris, R. V., Pike, W. T., Zent, A. P., 2009. Ground ice at the Phoenix landing site: Stability state and origin. *J. Geophys. Res.* 114, E00E07.
- Mellon, M. T., Jakosky, B. M., 1993. Geographic variations in the thermal and diffusive stability of ground ice on Mars. *J. Geophys. Res.* 98 (E2), 3345–3364.
- Mellon, M. T., Jakosky, B. M., 1995. The distribution and behavior of Martian ground ice during past and present epochs. *J. Geophys. Res.* 100 (E6), 11,781–11,799.
- Mellon, M. T., Jakosky, B. M., Postawko, S. E., 1997. The persistence of equatorial ground ice on Mars. *J. Geophys. Res.* 102 (E8), 19,357–19,369.
- Mischna, M. A., Richardson, M. I., Wilson, R. J., McCleese, D. J., 2003. On the orbital forcing of martian water and CO<sub>2</sub> cycles: A general circulation model study with simplified volatile schemes. *J. Geophys. Res.* E108, 5062.

- Mitrofanov, I. G., et al., 2002. Maps of subsurface hydrogen from the high-energy neutron detector, Mars Odyssey. *Science* 297 (5578), 78–81.
- Press, W. H., Teukolsky, S. A., Vetterling, W. T., Flannery, B. P., 1992. *Numerical Recipes in C* (Second ed.). Cambridge University Press, New York.
- Schorghofer, N., 2007a. Dynamics of ice ages on Mars. *Nature* 449 (7159), 192–194.
- Schorghofer, N., 2007b. Theory of ground ice stability in sublimation environments. *Phys. Rev. E* 75, 041201.
- Schorghofer, N., 2008a. The history of ice at the Phoenix Mars landing site. In: *Lunar & Planet. Sci. Conf.*, Volume 39. abstract # 1479.
- Schorghofer, N., 2008b. Temperature response of Mars to Milankovitch cycles. *Geophys. Res. Lett.* 35, L18201.
- Schorghofer, N., Aharonson, O., 2005. Stability and exchange of subsurface ice on Mars. *J. Geophys. Res.* 110 (E5), E05003.
- Sizemore, H. G., et al., 2010. In situ analysis of ice table depth variations in the vicinity of small rocks at the Phoenix Landing Site. *J. Geophys. Res.* 115, E00E09.
- Sizemore, H. G., Mellon, M. T., 2008. Laboratory characterization of the structural properties controlling dynamical gas transport in Mars analog soils. *Icarus* 197, 606–620.
- Smith, P. H., et al., 2009. H<sub>2</sub>O at the Phoenix Landing Site. *Science* 325 (5936), 58–61.
- Toon, O. B., Pollack, J. B., Ward, W., Burns, J. A., Bilski, K., 1980. The astronomical theory of climate change on Mars. *Icarus* 44, 552–607.
- van Everdingen, R. (Ed.), 1998. *Multi-Language Glossary of Permafrost and Related Ground-Ice Terms*. National Snow and Ice Data Center/World Data Center for Glaciology, Boulder, Colorado.